Geochemical Perspectives Letters

© 2022 The Authors
Published by the European Association of Geochemistry

Preservation of the isotope signatures in chondritic IOM during aqueous alteration

B. Laurent, L. Remusat, J.-C. Viennet, R. Brunetto, L. Binet, M. Holin, M. Ciocco, A. Brunelle, C. Bouvier. S. Bernard

Supplementary Information

The Supplementary Information includes:

- Sample Selection
- Experimental Procedure
- XANES Spectroscopy
- Raman Spectroscopy
- Infrared Spectroscopy
- TOF SIMS Mass Spectrometry
- Elemental Analysis
- NanoSIMS Mass Spectrometry
- EPR Spectroscopy
- Figures S-1 to S-4
- Table S-1
- Supplementary Information References

Sample Selection

The IOM of all chondrites were isolated by HF/HCl treatments as described in Vinogradoff *et al*. (2017) for Paris. Samples of Aguas Zarcas (Alajuela province, Costa Rica, 2019) and Mukundpura (Rajasthan, India, 2017) were provided by Luc Labenne. Initially, 4.4 and 6.3 g of bulk material were respectively separated and crushed using a stainless-steel mortar. The soluble fraction was isolated using successive extraction in

solvents, in Teflon vials, partly immersed in a sonicated H_2O bath. The extraction was performed using the protocol described in the Supplementary Information of Laurent *et al*. (2022).

Experimental Procedure

A starting mixture of 10 µL ultrapure water (produced by a Veolia Chorus 3 system, resistivity 18.2 MΩ and COT <3 ppb) and 10 µg of Paris IOM was loaded in pure gold capsule. The capsule was closed by arc welding, using Lampert pulse welder, set a 28mV and 5ms pulse, and loaded into a 23 mL PTFE reactor. The reactor was filled with 12 mL of the same ultrapure water, in order to work at conditions of water vapour saturation pressure (P_{sat} = 6 bars). The reactor was then put in an oven with temperature accurately regulated at 150 °C for 49 days. At the end of the experiment, the reactor was allowed to cool down freely. Capsule integrity afterwards was checked using optical microscope. The capsule was intact, and the solid residue was recovered by centrifugation, washed successively with ultrapure water, high grade ethanol, dichloromethane, and then air dried.

XANES Spectroscopy

For XANES data collection, the HERMES STXM beamline was operated at the synchrotron SOLEIL (Belkhou *et al.*, 2015; Swaraj *et al.*, 2017; Hitchcock, 2018). In order to prevent a carbon contamination, all the beamline's optical elements were exposed to a continuous flow of pure O_2. The 3p Rydberg peak of gaseous CO_2 at 294.96 eV was used for energy calibration. Image stacks were collected over the carbon absorption range (270–350 eV) at every 0.1 eV. The dwell time was set below 1ms, in order to any prevent irradiation damages (Wang *et al.*, 2009). From the method described in Le Guillou *et al.* (2018), the background of XANES spectra was subtracted using a power law, and the integration of the signal from the pre-edge region up to the mean ionisation energy (*e.g.*, 282.0–291.5 eV at the C K edge) allowed the normalisation of each spectrum to the carbon quantity and the quantification of functional group concentrations (Le Guillou *et al.*, 2018).

Raman Spectroscopy

Raman Spectra were acquired using a Renishaw InVia spectrometer, associated with an argon laser (514.5 nm) for a nominal power of 36 mW. To prevent any laser-induced heating, the laser was used at 0.1 % of its power, yielding a planar resolution of ~ 2 µm for a power of less than 10 µW delivered at the sample surface. For laser power >0.1 %, clear indication of laser-induced heating was observed, with a shift of the G band towards low wavenumbers (Fig. S-4). Data were collected by averaging 500 accumulations on a static range between 500 and 2000 cm^{-1}. Linear shaped baseline between 1000 and 1900 cm^{-1} was applied, using the Fityk software (Wojdyr 2010). The peak deconvolution utilises 5 Gaussians at fixed position, to measure the evolution of the different defect bandwidths in regard to the hydrothermal alteration. Main G and D bands were set at 1595 and 1355 cm^{-1}, and the minor defect bands named $D_{1,2,4}$ were respectively fixed at 1200, 1500 and 1620 cm^{-1}. Standard deviations are given by the covariance value (%) between the spectra and their fit, and calculated from the weighted sum squared residual (WSSR).

Infrared Spectroscopy

Infrared spectra were collected on IOM samples deposited on IR transparent CaF2 windows at the SMIS beamline of the SOLEIL synchrotron (France) using an Agilent Cary 670/620 micro-spectrometer equipped with a 128x128 pixel Focal Plane Array detector (3900–800 cm^{-1}) and with a single point MCT detector (6000–650 cm^{-1}). MCT detector was used and the internal globar source at 4 cm^{-1} spectral resolution. The micro-IR spectra were acquired in transmittance geometry (256 accumulated scans per sample), with respect to clean CaF2 areas, using a x25 objective and 80 µm spot size on the focal plane. Measurements were performed using KBr pellets. Using Fityk software, IR spectra were baseline corrected using a spline functions, with 6 anchor points at 740, 820, 920, 1270, 3600, 4000 cm^{-1}. Gaussian fit was applied, at fixed positions (1040, 1245, 1385, 1450, 1590 and 1710 cm^{-1}). Aromatic C-H are taken at 1590 cm^{-1}, and aliphatic C-C were taken at 1385 and 1450 cm^{-1} (mean values reported here), and C-O at 1710 cm^{-1}. For the CH_2/CH_3 determination, additional linear fit was applied between 2700 and 3100 cm^{-1}, and fitting was obtained using 4 fixed gaussians at 2850, 2870, 2920 (CH_2) and 2960 (CH_3) cm^{-1}. Standard deviations are given by the covariance value (%) between the spectra and their fit, and calculated from the weighted sum squared residual (WSSR).

TOF SIMS Mass Spectrometry

The Time-of-Flight mass spectrometry analysis was performed on the TOF-SIMS IV (IONTOF GmbH, Germany) at the Laboratory of Molecular and Structural Archaeology (LAMS, CNRS – Sorbonne University, Paris, France). The primary ion source used for analysis was a liquid metal ion gun delivering a bismuth cluster pulsed ion beam (25 keV energy Bi_3^+ ions) hitting the surface with an incidence angle of 45°, with a low energy electron flood gun neutralising the surface between each analysis scan. The time-of-flight analyser is equipped with delayed extraction of secondary ions, which offers the possibility of coupling a high spatial resolution with a mass resolution of a few thousand (M/ΔM, full width at half maximum). The analyses were then made using this so-called "burst alignment with delayed extraction" (BA+DE) focusing mode. The beam diameter can be reduced down to 400 nm because the long primary ion pulses (~100 ns) are compensated by the delayed extraction (DE) of the secondary ions (full description given by Vanbellingen *et al.*, 2015). The primary dose was 5.10^{12} ions/cm². Before the analysis, a 500 µm side square around the analysed areas was cleaned with a dose of 2 to 4.10^{14} ions/cm² using 10 keV argon clusters of 2000 atoms emitted by a Gas Cluster Ion Beam (GCIB), which allows a gentle sputtering of the surface without damaging the underlying layers, to remove surface contamination. Raw data were acquired using SurfaceLab 6.7 software (IONTOF GmbH, Germany) and processed with SurfaceLab 7.0. A typical statistical error was applied using the quadratic sum of signal intensities.

Elemental Analysis

The bulk H-isotope measurements for Aguas Zarcas and Mukundpura were performed on an Elementar VisION interfaced with an Elementar pyrocube. About 1 mg of IOM were loaded into silver capsules. Capsules were stored in an autosampler set at 80 °C, then dropped into a 1450 °C furnace made in glassy carbon, and flushed by pure He. The instrument reproducibility and bias were checked using the CH_7 polyethylene standard from IAEA. Measurements were made in replicates.

NanoSIMS Mass Spectrometry

The Cameca NanoSIMS 50 (MNHN, Paris) was acquiring δD and d15N images of IOMs, in two sessions. Pressed samples onto clean indium foil were gold coated (final 20 nm thick). Secondary ions of H^- and D^- were collected to obtain δD images and ^{16}O-, $^{12}C^{2-}$, $^{26}CN^-$, $^{27}CN^-$ and ^{32}S- for $\delta^{15}N$ images. To minimise topographic effects on IOM N/C measurements, $^{26}CN^-/^{12}C^{2-}$ was the ion ratio measured (Thomen *et al.*, 2014). Prior to any analysis, a 25×25 μm² pre-sputtering was applied, for a duration of 10 minutes and using a 300 pA primary current. Its role was to remove the sample coating, clean the surface and to reach a sputtering steady state. For H and N isotopes, the primary Cs^+ beam (16 keV) was set at 14 pA and 2 pA. The resulting spatial resolution was 300 and 150 nm, for hydrogen and nitrogen respectively. Image collection was set 256×256 pixel covering 20×20 μm², with a raster speed of 1ms/pix. Electron multipliers were used, with a dead time of 44 ns in multicollection mode. The resulting mass resolving power was set at 5000 (for H) and for N isotopes it was increased to 9000, to resolve interferences such as $^{12}C^{15}N^-$ from $^{13}C^{14}N^-$ and $^{32}S^-$ from $^{16}O^{2-}$. The vacuum was consistently below 5×10^{-10} torr. All NanoSIMS data were processed with L'image software (Larry Nittler, Carnegie Institution in Washington DC, USA). Isotopic ratio and the elemental ratios were corrected using calibration lines, by measuring known reference samples: terrestrial type 3 kerogen from Virginia and charcoal as well as the IOM of Orgueil meteorites (Remusat *et al.*, 2016).

Uncertainties are 1 sigma errors, combining counting statistics uncertainties on each measurement and uncertainties from the calibration lines. Isotopic ratios are expressed in delta units, following the relation:

$$\delta\ (‰) = (R_{sple}/R_{std}-1) \times 1000$$

with R_{sple} being the sample isotopic ratio and R_{std} the ratio of a terrestrial standard; Standard Mean Ocean Water (SMOW: D/H= 155.76×10^{-6}) for H isotopes and Air for N ($^{15}N/^{14}N= 3.67 \times 10^{-3}$).

EPR Spectroscopy

The EPR spectra were recorded with a Bruker Elexsys E500 spectrometer operating at X-band (microwave frequency ≈9.4 GHz), equipped with an 4122SHQE resonator and an Oxford ESR900 helium flow cryostat for sample cooling. A modulation of the magnetic field at 100 kHZ with a 0.1 mT amplitude was applied for lock-in detection of the EPR spectra. The applied microwave power was 64 μW, low enough to avoid saturation. Samples masses were 12.0 mg and 10.5 mg for AZ and MK samples, respectively. The spectra were recorded with the samples under vacuum, with a residual pressure $\leq 10^{-3}$ mbar. The intensities of the spectra were calculated from $A \times (\Delta B)^2$ where A is the peak-to-peak height and ΔB the peak-to-peak width of the EPR line.

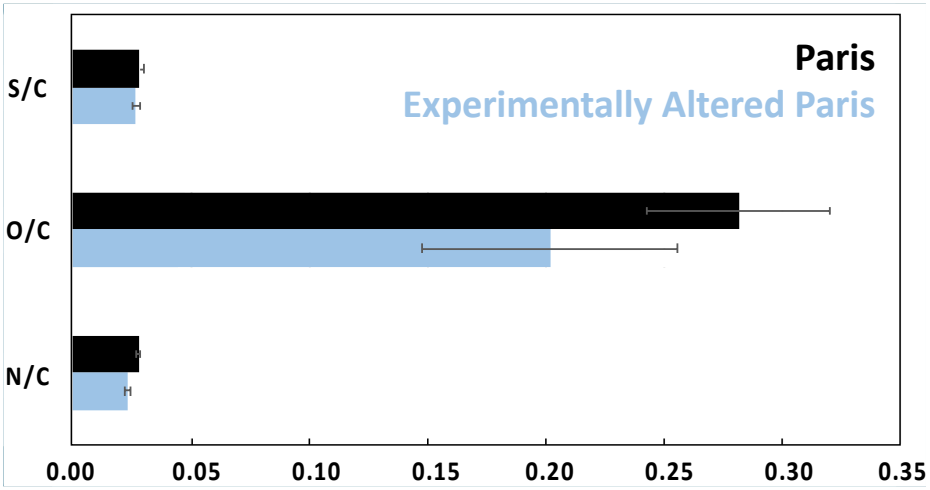

Figure S-1 Evolution of elemental ratios. Comparison of S/C, O/C and N/C from NanoSIMS analysis of experimentally altered Paris H2O (blue) and Paris (black). For respectively Paris and the experimental residue, N/C = 2.8±0.1 and 2.3±0.1, O/C = 28.2±4.0 and 20.2±5.4, S/C = 2.8±0.2 and 2.7±0.1.

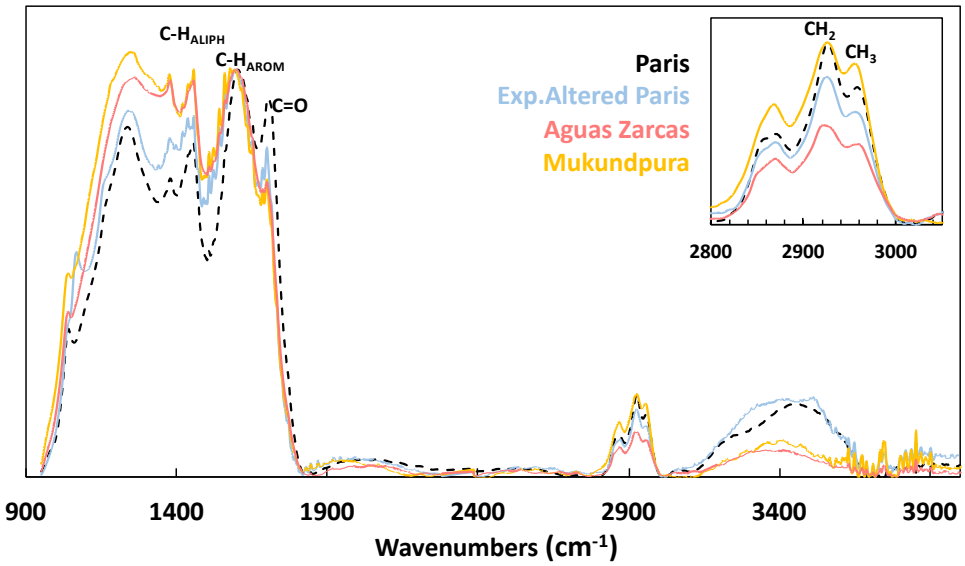

Figure S-2 Infrared absorbance spectra of Paris (black), the experimentally altered Paris ('Altered Paris', blue), and altered CM2 Aguas Zarcas (pink) and Mukundpura (yellow), normalised to the C-H$_{aromatic}$ intensity. The black box is centred around the C-H stretch aliphatic area.

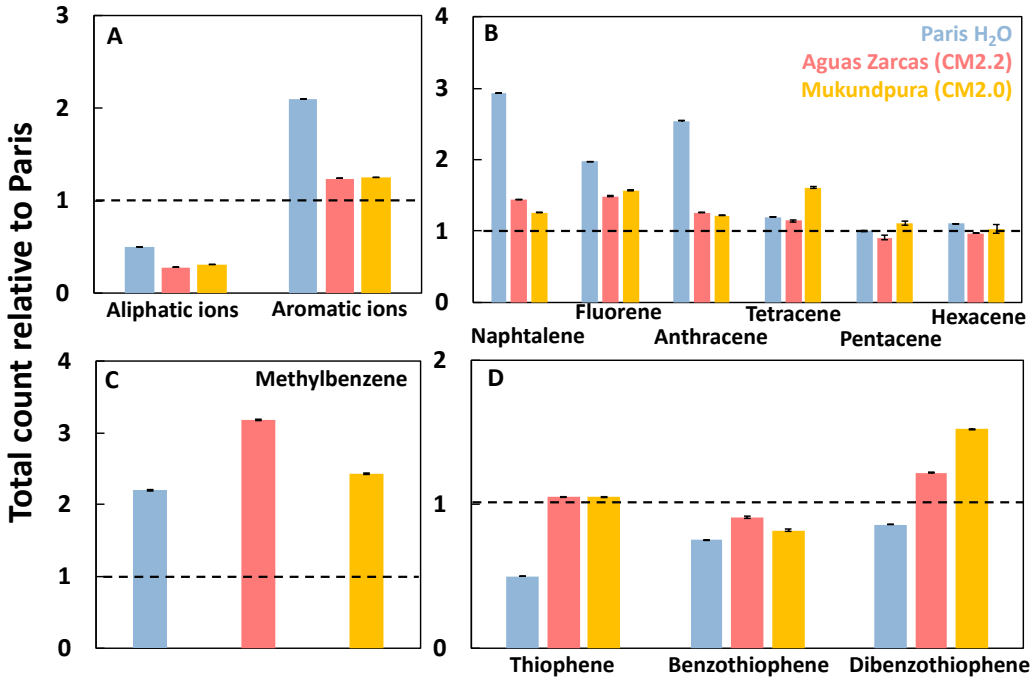

Figure S-3 Comparison between experimentally altered IOM from Paris and recently recovered CM2 TOFF-SIMS data. **(a)** Relative Intensity of secondary aliphatic and aromatic ions, normalised to total carbon signal for PAHs, for experimentally altered Paris (blue), CM2.2 Aguas Zarcas (pink) and CM2.0 Mukundpura (yellow). **(b,c,d)** Idem for respectively PAHs, methylbenzene and thiophenic compounds. Mass and formula associated with detected fragments are reported on Table S-1 below.

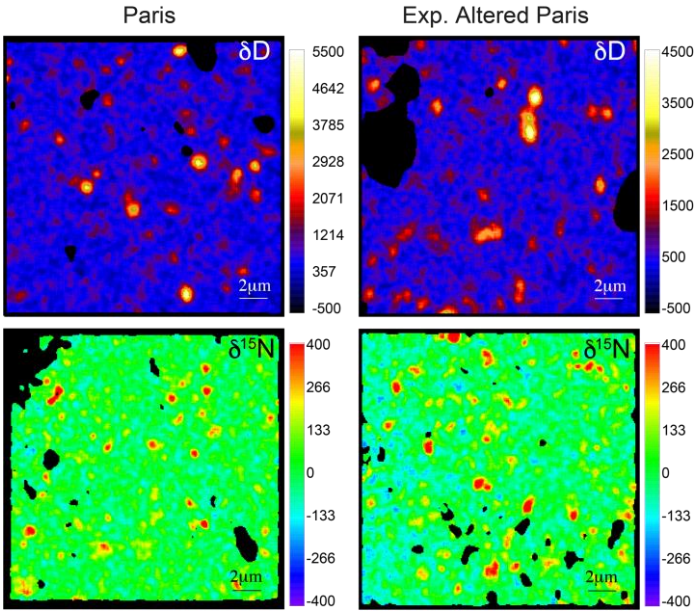

Figure S-4 Nitrogen and hydrogen hotspot distribution. NanoSIMS images of H-isotope and N-isotope distribution in Paris (left) and experimentally altered Paris (right), each image covers a surface of 20 x 20 µm^2.

Table S-1 Name, Mass and formula associated with detected carbon fragments in TOF SIMS.

Molecular fragment	Formula	Mass
methylbenzene	$C_7H_8^+$	92.1
thiophene	$C_4H_4S^+$	84.1
benzotiophene	$C_8H_6S^+$	134.1
dibenzotiophene	$C_{12}H_8S^+$	184.2
methylbenzene	$C_7H_8^+$	92.1
Aromatic ions		
naphtalene	$C_{10}H_8^+$	128.1
fluorene	$C_{13}H_{10}^+$	166.1
anthracene	$C_{14}H_{10}^+$	178.2
tetracene	$C_{18}H_{12}^+$	228.3
perylene	$C_{20}H_{12}^+$	252.2
pentacene	$C_{22}H_{14}^+$	278.2
hexacene	$C_{26}H_{16}^+$	328.5
coronene	$C_{24}H_{12}^+$	300.2
heptacene	$C_{30}H_{10}^+$	378.3
Aliphatic ions		
ethylene	$C_2H_4^+$	28.0
ethane	$C_2H_6^+$	30.0
cyclopropane	$C_3H_6^+$	42.1
cyclobutenyl	$C_4H_3^+$	51.1
isobutylene	$C_4H_8^+$	56.0
pentane	$C_5H_{12}^+$	72.1

Supplementary Information References

Belkhou, R., Stanescu, S., Swaraj, S., Besson, A., Ledoux, M., Hajlaoui, M., Dalle, D. (2015) HERMES: a soft X-ray beamline dedicated to X-ray microscopy. *Journal of Synchrotron Radiation* 22, 968–979. https://doi.org/10.1107/S1600577515007778

Hitchcock, A.P. (2018) Influence of local environment on inner shell excitation spectra, studied by electron and X-ray spectroscopy and spectromicroscopy. *Zeitschrift für Physikalische Chemie* 232, 723–745. https://doi.org/10.1515/zpch-2017-1061

Laurent, B., Maillard, J., Afonso, C., Danger, G., Giusti, P., Remusat, L. (2022) Diversity of chondritic organic matter probed by ultra-high resolution mass spectrometry. *Geochemical Perspectives Letters* 22, 31–35. https://doi.org/10.7185/geochemlet.2224

Le Guillou, C., Bernard, S., De la Pena, F., Le Brech, Y. (2018) XANES-based quantification of carbon functional group concentrations. *Analytical Chemistry* 90, 8379–8386. https://doi.org/10.1021/acs.analchem.8b00689

Remusat, L., Piani, L., Bernard, S. (2016) Thermal recalcitrance of the organic D-rich component of ordinary chondrites. *Earth and Planetary Science Letters* 435, 36–44. https://doi.org/10.1016/j.epsl.2015.12.009

Swaraj, S., Belkhou, R., Stanescu, S., Rioult, M., Besson, A., Hitchcock, A.P. (2017) Performance of the HERMES beamline at the carbon K-edge. *Journal of Physics: Conference Series* 849, 012046.

Thomen, A., Robert, F., Remusat, L. (2014) Determination of the nitrogen abundance in organic materials by NanoSIMS quantitative imaging. *Journal of Analytical Atomic Spectrometry* 29, 512-519. https://doi.org/10.1039/C3JA50313E

Vanbellingen, Q. P., Elie, N., Eller, M. J., Della-Negra, S., Touboul, D., Brunelle, A. (2015) Time-of-flight secondary ion mass spectrometry imaging of biological samples with delayed extraction for high mass and high spatial resolutions. *Rapid Communications in Mass Spectrometry 29*, 1187–1195. https://doi.org/10.1002/rcm.7210

Vinogradoff, V., Le Guillou, C., Bernard, S., Binet, L., Cartigny, P., Brearley, A.J., Remusat, L. (2017) Paris vs. Murchison: Impact of hydrothermal alteration on organic matter in CM chondrites. *Geochimica et Cosmochimica Acta* 212, 234–252. https://doi.org/10.1016/j.gca.2017.06.009

Wang, J., Morin, C., Li, L., Scholl, A., Doran, A. (2009) Radiation damage in soft X-ray microscopy. Journal of Electron Spectroscopy and Related Phenomena 170, 25–36. https://doi.org/10.1016/j.elspec.2008.01.002

Wojdyr, M. (2010) Fityk: a general-purpose peak fitting program. *Journal of Applied Crystallography* 43, 1126–1128. https://doi.org/10.1107/S0021889810030499